ISSN 1560-3547, Regular and Chaotic Dynamics, 2015, Vol. 20, No. 5, pp. 605–626. © Pleiades Publishing, Ltd., 2015.

Dynamics of the Suslov Problem in a Gravitational Field: Reversal and Strange Attractors

Ivan A. Bizyaev[1,2*], Alexey V. Borisov[2], and Alexey O. Kazakov[1,3***]**

[1] *Udmurt State University, ul. Universitetskaya 1, Izhevsk, 426034 Russia*

[2] *Steklov Mathematical Institute, Russian Academy of Sciences, ul. Gubkina 8, Moscow, 119991 Russia*

[3] *National Research University Higher School of Economics, ul. Rodionova 136, Nizhny Novgorod, 603093 Russia*

Received August 14, 2015; accepted September 17, 2015

Abstract—In this paper, we present some results on chaotic dynamics in the Suslov problem which describe the motion of a heavy rigid body with a fixed point, subject to a nonholonomic constraint, which is expressed by the condition that the projection of angular velocity onto the body-fixed axis is equal to zero. Depending on the system parameters, we find cases of regular (in particular, integrable) behavior and detect various attracting sets (including strange attractors) that are typical of dissipative systems. We construct a chart of regimes with regions characterizing chaotic and regular regimes depending on the degree of conservativeness. We examine in detail the effect of reversal, which was observed previously in the motion of rattlebacks.

MSC2010 numbers: 37J60, 37N15, 37G35, 70E18, 70F25, 70H45

DOI: 10.1134/S1560354715050056

Keywords: Suslov problem, nonholonomic constraint, reversal, strange attractor

Contents

*E-mail: bizaev_90@mail.ru

**E-mail: borisov@rcd.ru

***E-mail: kazakovdz@yandex.ru

1. INTRODUCTION

We note that the recently increased interest in problems of nonholonomic mechanics is due, first, to the development of new methods of numerical analysis and, second, to a great importance of such problems for applications in mobile robotics.

For more on the stages of historical development of nonholonomic mechanics see, for example, [1]. Here we would only like to note that systems of nonholonomic mechanics exhibit a greater variety of dynamical behaviors than Hamiltonian systems [2]. This variety of behaviors stems, on the one hand, from the presence (or absence) of various *tensor invariants* in the system (such as first integrals, invariant measure, and Poisson structure) and, on the other hand, from the *reversibility* of the system and the number and type of *involutions*.

As an example of the variety of behaviors in nonholonomic systems we consider two particularly interesting problems which are fundamentally different from a dynamical point of view: the Chaplygin ball rolling problem [3] and the problem of motion of a rattleback [4, 5]. The former is described by an integrable system, while the latter is nonintegrable and, moreover, exhibits strange attractors [6, 7].

In this paper we consider the nonholonomic Suslov problem describing the motion of a heavy rigid body with a fixed point, subject to a nonholonomic constraint, which is expressed by the condition that the projection of angular velocity onto the body-fixed axis is equal to zero. For convenience, we call such a body the *Suslov top*.

In the problem considered here we find integrable cases and cases of existence of an invariant measure. The inertial motion of a rigid body was studied by Suslov [8] and Vagner [9] and in more recent works [10–12], from which it is known that under certain restrictions to the moments of inertia of the body the system possesses an invariant measure with constant density and, in the general case, a measure with singular density (i.e., having singularities at certain points of phase space).

In the present paper we show that in the general case (in a gravitational field) the Suslov problem does not possess an invariant measure. In this case, in the phase space of the system (depending on parameters) there can exist different limiting regimes ranging from regular attractors (which are not always expressed in terms of quadratures) to strange attractors.

In Section 2 we present equations of motion for the Suslov top and find first integrals. In Section 3 we consider various particular cases in which the system possesses additional first integrals and an invariant measure. In Section 4 we describe the procedure of constructing a Poincaré map for numerical analysis of the system and present a complete list of involutions in the system.

Section 5 contains results on the "regular" dynamics of the Suslov top which are related to the existence of stable and unstable (due to reversibility) equilibria in the system, to which in absolute space there correspond rotations of the Suslov top about the vertical axis. Owing to the presence of stable and unstable equilibria the top can execute a *reversal*. We recall that the reversal of a rigid body is understood to mean a change in the direction of the body's rotation when the trajectories pass from a neighborhood of an unstable equilibrium to a stable one. The phenomenon of reversal was first discovered in rattleback dynamics [4, 5]. Quite recently the reversal has been detected in the nonholonomic model describing the motion of the Chaplygin top (a dynamically asymmetric ball with a displaced center of mass [13]). In Section 5.3 we show that for the Suslov top the phenomenon of reversal can be of two types: like that of a rattleback, when the body reverses the direction of rotation about the vertical axis, or like that of the Thompson top [14] (or a dynamically asymmetric ellipsoid of revolution [15]), when the axis of rotation of the body turns over. It can be said that one of the results of this paper is the observation that reversal is a fairly universal property of nonholonomic systems (see also [16]).

Section 6 presents results on chaotic dynamics, which have been obtained by analyzing the charts of Lyapunov exponents, and introduces numerical criteria for the classification of chaotic dynamics.

This criterion made it possible to show that in addition to simple attractors and repellers (by virtue of reversibility) and complex strange attractors, the system has zones in which due to reversibility the behavior of the system is close to conservative (more detailed analyses of such zones using the construction of involutive networks were carried out previously in [17, 31]). In the conclusion of Section 6 we construct a chart of Lyapunov exponents, when the (two-dimensional) Poincaré map possesses no involutions, describe equilibrium bifurcations of the system and show that the system can have strange attractors of Feigenbaum type [37].

In Section 7 we consider the Suslov problem in the case of an inhomogeneous constraint. As a rule, in this case there is no energy integral. We present a new case of integrability (the generalizing Kozlov case for a homogeneous constraint) and show that in the general case the problem reduces to the investigation of an (essentially) three-dimensional Poincaré map (i.e., when two additional integrals are absent).

The dynamics have been explored using the software package "Computer dynamics: Chaos", which was developed at the Institute of Computer Science of the Udmurt State University and which allows one to construct charts of regimes and charts of Lyapunov exponents, to investigate bifurcations of fixed points and to visualize the motion of the body. Highly efficient numerical experiments were conducted using the software package "Computer Dynamics: Chaos" by means of a computational cluster of the laboratory LATNA of the National Research University Higher School of Economics.

2. EQUATIONS OF MOTION

Consider the motion of a heavy rigid body with a fixed point in the presence of the nonholonomic constraint

$$(\boldsymbol{\omega}, \boldsymbol{e}) = 0, \tag{2.1}$$

where $\boldsymbol{\omega}$ is the angular velocity of the body and $\boldsymbol{e}$ is the unit vector fixed in the body.

The constraint (2.1) was introduced by G. K. Suslov in [8, p. 593]. The realization of the constraint (2.1) by means of wheels with sharp edges rolling over a fixed sphere was proposed by V. Vagner [9] (see Fig. 1). The sharp edges of the wheels prevent the wheels from sliding in the direction perpendicular to their plane.

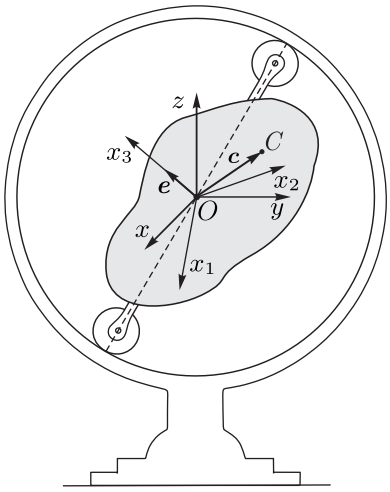

Fig. 1. Realization of the Suslov problem.

Choose two coordinate systems:

— *an inertial* (fixed) coordinate system $Oxyz$;

— *a noninertial* (moving) coordinate system $Ox_1x_2x_3$ rigidly attached to the rigid body in such a way that $Ox_3 \| \boldsymbol{e}$ and the axes Ox_1 and Ox_2 are directed so that one of the components of the tensor of inertia of the body vanishes: $I_{12} = 0$.

To parameterize the configuration space, we choose a matrix of the direction cosines $\mathbf{Q} \in SO(3)$ the columns of which contain the unit vectors $\boldsymbol{\alpha}$, $\boldsymbol{\beta}$ and $\boldsymbol{\gamma}$ of the fixed axes Ox, Oy and Oz projected onto the axes of the moving coordinate system $Ox_1x_2x_3$

$$\mathbf{Q} = \begin{pmatrix} \alpha_1 & \beta_1 & \gamma_1 \\ \alpha_2 & \beta_2 & \gamma_2 \\ \alpha_3 & \beta_3 & \gamma_3 \end{pmatrix} \in SO(3).$$

In the moving coordinate system $Ox_1x_2x_3$ the constraint equation (2.1) and the tensor of inertia $\mathbf{I}$ of the rigid body have the form

$$\omega_3 = 0, \qquad \mathbf{I} = \begin{pmatrix} I_{11} & 0 & I_{13} \\ 0 & I_{22} & I_{23} \\ I_{13} & I_{23} & I_{33} \end{pmatrix}. \tag{2.2}$$

Let $\boldsymbol{c} = (c_1, c_2, c_3)$ be the vector of displacement of the center of mass of the body relative to the fixed point O and assume that the entire system is in a gravitational field with the potential

$$U = (\boldsymbol{b}, \boldsymbol{\gamma}), \quad \boldsymbol{b} = -m\mathrm{g}\boldsymbol{c},$$

where m is the mass of the rigid body and g is the free fall acceleration.

The equations of motion for $\boldsymbol{\omega}$ in the moving coordinate system $Ox_1x_2x_3$ have the form

$$\begin{gathered} \mathbf{I}\dot{\boldsymbol{\omega}} = \mathbf{I}\boldsymbol{\omega} \times \boldsymbol{\omega} + \lambda \boldsymbol{e} + \boldsymbol{\gamma} \times \frac{\partial U}{\partial \boldsymbol{\gamma}}, \\ \lambda = -\frac{\left(\mathbf{I}\boldsymbol{\omega} \times \boldsymbol{\omega} + \boldsymbol{\gamma} \times \frac{\partial U}{\partial \boldsymbol{\gamma}}, \mathbf{I}^{-1}\boldsymbol{e}\right)}{(\boldsymbol{e}, \mathbf{I}^{-1}\boldsymbol{e})}, \end{gathered} \tag{2.3}$$

where $\boldsymbol{e} = (0, 0, 1)$.

Adding to the system (2.3) the kinematic Poisson equations governing the evolution of the unit vectors $\boldsymbol{\alpha}$, $\boldsymbol{\beta}$, and $\boldsymbol{\gamma}$:

$$\dot{\boldsymbol{\alpha}} = \boldsymbol{\alpha} \times \boldsymbol{\omega}, \quad \dot{\boldsymbol{\beta}} = \boldsymbol{\beta} \times \boldsymbol{\omega}, \quad \dot{\boldsymbol{\gamma}} = \boldsymbol{\gamma} \times \boldsymbol{\omega}, \tag{2.4}$$

we obtain a complete system governing the motion of the rigid body.

In Eqs. (2.3) and (2.4), a closed system for the variables $(\omega_1, \omega_2, \gamma_1, \gamma_2, \gamma_3)$ decouples. In view of the constraint (2.2) this system can be represented as

$$\begin{aligned} I_{11}\dot{\omega}_1 &= -\omega_2(I_{13}\omega_1 + I_{23}\omega_2) + b_3\gamma_2 - b_2\gamma_3, \\ I_{22}\dot{\omega}_2 &= \omega_1(I_{13}\omega_1 + I_{23}\omega_2) + b_1\gamma_3 - b_3\gamma_1, \\ \dot{\gamma}_1 &= -\gamma_3\omega_2, \\ \dot{\gamma}_2 &= \gamma_3\omega_1, \\ \dot{\gamma}_3 &= \gamma_1\omega_2 - \gamma_2\omega_1. \end{aligned} \tag{2.5}$$

The system (2.5) possesses an energy integral and a geometric integral:

$$E = \frac{1}{2}(I_{11}\omega_1^2 + I_{22}\omega_2^2) + (\boldsymbol{b}, \boldsymbol{\gamma}), \quad F_1 = \boldsymbol{\gamma}^2 = 1. \tag{2.6}$$

Thus, on the fixed level set of the energy integral $E = h$ and $F_1 = 1$ the system (2.5) defines the flow on the three-dimensional manifold $\mathcal{M}_h^3$:

$$\mathcal{M}_h^3 = \{(\omega_1, \omega_2, \gamma_1, \gamma_2, \gamma_3), \mid E = h, \ F_1 = 1\},$$

for it to be integrable by the Euler – Jacobi theorem [19], an additional first integral F_2 and an invariant measure are necessary.

In order to reconstruct the motion of the rigid body in the fixed coordinate system $Oxyz$ from the known solutions $\boldsymbol{\omega}(t)$ and $\boldsymbol{\gamma}(t)$ of (2.5), we have to define $\boldsymbol{\alpha}$ and $\boldsymbol{\beta}$ from the system (2.4), which reduces to an equation for the precession angle ψ, i.e., to the quadrature

$$\dot{\psi} = \frac{\omega_1(t)\gamma_1(t) + \omega_2(t)\gamma_2(t)}{\gamma_1^2(t) + \gamma_2^2(t)}. \tag{2.7}$$

Therefore, the properties of the resulting system (2.5) determine in many respects the properties of the dynamics of the entire system.

3. FIRST INTEGRALS AND INVARIANT MEASURE

Depending on the type of the tensor of inertia and the displacement of the center of mass of the rigid body, the system (2.5) can possess an additional first integral and a (possibly singular) invariant measure. In this section we shall consider the following particular cases:

— a balanced rigid body ($\boldsymbol{b} = 0$) for which $I_{13}^2 + I_{23}^2 \neq 0$;

— an unbalanced rigid body ($\boldsymbol{b} \neq 0$) in which $\boldsymbol{e}$ is directed along one of the principal axes of inertia of the body: $I_{13} = I_{23} = 0$;

— an unbalanced rigid body ($\boldsymbol{b} \neq 0$) for which $I_{13}^2 + I_{23}^2 \neq 0$.

3.1. A Balanced Rigid Body ($\boldsymbol{b} = 0$)

In the system (2.5) the equations for the angular velocities ω_1 and ω_2 decouple. The phase portrait on the fixed level set of the energy integral $E = h$ is shown in Fig. 2, in which the straight line $I_{13}\omega_1 + I_{23}\omega_2 = 0$ is entirely filled with fixed points.

On each level set of the energy integral there are two (isolated) fixed points, one of them is asymptotically stable and the other is asymptotically unstable (see, e.g., [10]).

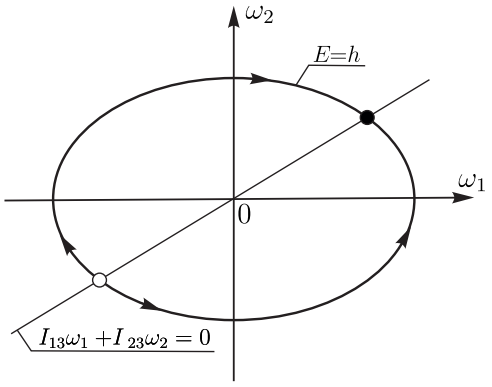

Fig. 2. A typical phase portrait of the system (2.5).

Due to asymptotic behavior the system (2.5) possesses in this case an invariant measure with singular density [10]

$$\rho = (I_{13}\omega_1 + I_{23}\omega_2)^{-1}.$$

Explicitly integrating, we find

$$\omega_1(t) = \frac{\omega_0 I_{22}}{I_{11}I_{23}^2 + I_{22}I_{13}^2}\,\frac{2I_{13}\sqrt{I_{11}I_{22}}e^{\omega_0 t} \pm I_{11}I_{23}(1-e^{2\omega_0 t})}{1+e^{2\omega_0 t}},$$
$$\omega_2(t) = \frac{\omega_0 I_{11}}{I_{11}I_{23}^2 + I_{22}I_{13}^2}\,\frac{2I_{23}\sqrt{I_{11}I_{22}}e^{\omega_0 t} \pm I_{22}I_{13}(1-e^{2\omega_0 t})}{1+e^{2\omega_0 t}}, \tag{3.1}$$
$$h = \frac{I_{11}^2 I_{22}^2 \omega_0^2}{I_{11}I_{23}^2 + I_{22}I_{13}^2}.$$

For the known $\omega_1(t)$ and $\omega_2(t)$ the unit vector $\boldsymbol{\gamma}$ is defined according to (2.5) by a linear nonautonomous system of equations, which by a complex change of variables reduces to the Riccati equation (see, e.g., [9]). However, in the general case its solution bifurcates on the complex plane of time [20] and hence is not represented in quadratures.

In [10] it is noted that under the following restrictions on the moments of inertia:

$$I_{13} = 0, \quad I_{11} = I_{22} + \frac{I_{23}^2}{I_{22}}k^2, \quad \text{where} \quad k = 2n+1, \quad n \in \mathbb{Z} \tag{3.2}$$

the system (2.5) admits the additional integral F_2 [10]

$$F_2 = f_1^{(k)}(\omega_1,\omega_2)\gamma_1 + f_2^{(k)}(\omega_1,\omega_2)\gamma_2 + f_3^{(k)}(\omega_1,\omega_2)\gamma_3,$$

where the coefficients $f_1^{(k)}$, $f_2^{(k)}$ and $f_3^{(k)}$ are polynomials of odd degree k in the velocities ω_1 and ω_2. For example, for $k = 1$ we obtain

$$f_1^{(1)} = \left(I_{22} + \frac{I_{23}^2}{I_{22}}\right)\omega_1, \quad f_2^{(1)} = I_{22}\omega_2, \quad f_3^{(1)} = I_{23}\omega_2.$$

An explicit solution of $\boldsymbol{\gamma}(t)$ in this case was obtained in [11].

Let us describe the motion of the rigid body in absolute space, i.e., in the fixed coordinate system $Oxyz$. The fixed points of the system (2.5) in $Oxyz$ correspond to steady rotations about $\boldsymbol{\omega}$. All the other motions of the rigid body are transitions from one unstable steady rotation to another stable one. The connection of such an asymptotic problem with the phenomenon of reversal is shown in [21], where analogous effects in other nonholonomic problems are discussed.

In this case the axis of rotation rotates through some angle $\Delta\Phi$, which turns out to be independent of energy and for $I_{13} = 0$ is defined by [11]:

$$\cos\left(\frac{\Delta\Phi}{2}\right) = \frac{\cos\left(\frac{\pi}{2}k\right)}{\cosh\left(\frac{\pi}{2}\frac{I_{22}}{I_{23}}\right)}, \quad k^2 = \frac{I_{22}}{I_{23}}(I_{11} - I_{22}). \tag{3.3}$$

Thus, for odd k, i.e., when the above-mentioned integral exists, the axis of rotation reverses direction: $\Delta\Phi = \pm\pi$.

3.2. An Unbalanced Heavy Rigid Body ($\boldsymbol{b} \neq 0$)

Suppose that the center of mass of the rigid body does not coincide with the geometrical center of the shell (i.e., $\boldsymbol{b} \neq 0$). In this case, the system (2.5) can be called the *Suslov top* (by analogy with the Lagrange top).

As shown in [12], a necessary and sufficient condition for the existence of an invariant measure is $I_{13}^2 + I_{23}^2 = 0$. Consider the conditions for the existence of an additional integral in the presence and in the absence of an invariant measure.

Case $\mathbf{I_{13} = I_{23} = 0}$. The system (2.5) preserves a standard invariant measure ($\rho = \text{const}$), and the additional integral F_2 has been found in two cases:

— the Kharlamova case ($b_3 = 0$) [22] and $F_2 = I_{11}b_1\omega_1 + I_{22}b_2\omega_2$;

— the Kozlov case ($b_1 = b_2 = 0$, $I_{22} = I_{11}$) [12] and $F_2 = \omega_1\gamma_1 + \omega_2\gamma_2$.

In [23] it was proved that if the center of mass is displaced only along Ox_3 (i.e., $b_1 = b_2 = 0$, $b_3 \neq 0$), an additional meromorphic integral exists only for $I_{22} = I_{11}$. The absence of an additional meromorphic integral under more general restrictions on $\boldsymbol{b}$ was proved in [24, 25]).

Remark. The Suslov problem with $I_{13} = 0$ and $I_{23} = 0$, but in different integrable potential fields $U = U(\gamma_1, \gamma_2)$ possesses unusual topological properties, which are described in [10, 26–28], and the two-dimensional integral manifolds can have genus $g > 2$, i.e., they are no tori. In this case the equations of motion can be represented in Hamiltonian form, after rescaling time as $dt = \gamma_3^{-1} d\tau$, which is undefined for $\gamma_3 = 0$.

Case $\mathbf{I_{13}^2 + I_{23}^2 \neq 0}$. Here we present a new case in which there exists the additional integral F_2. In this case the system is nonintegrable by the Euler – Jacobi theorem, but its dynamics are regular.

If the components of the tensor of inertia and the displacement of the center of mass satisfy the relations

$$\begin{gathered} I_{13} = 0, \quad I_{23}^2 - I_{22}(I_{11} - I_{22}) = 0, \\ b_1 = 0, \quad I_{22} b_2 + I_{23} b_3 = 0, \end{gathered} \tag{3.4}$$

then the system (2.5) possesses the additional integral

$$F_2 = (I_{22}^2 + I_{23}^2)\gamma_1\omega_1 + I_{22}(I_{22}\gamma_2 + I_{23}\gamma_3)\omega_2.$$

We note that the family (3.4) is simultaneously a generalization of the family (3.2) for $k = 1$ and of the Kozlov case.

Thus, for (3.4) the system (2.5) defines the flow without a smooth invariant measure on some two-dimensional manifold

$$\mathcal{M}^2_{h,f} = \{(\omega_1, \omega_2, \gamma_1, \gamma_2, \gamma_3) \mid E = h,\ F_1 = 1,\ F_2 = f\}.$$

Remark. Flows on the two-dimensional manifold without a smooth invariant measure were also found in other nonholonomic systems (see, e.g., [29, 30]).

The question of the topological type of $\mathcal{M}^2_{h,f}$ and the structure of the bundle defined by the integrals H, F_1 and F_2 remains open.

4. THE POINCARÉ MAP AND INVOLUTIONS

In the general case, Eqs. (2.5) define the flow $\mathcal{F}$ on the three-dimensional manifold

$$\mathcal{M}^3_h = \{(\omega_1, \omega_2, \gamma_1, \gamma_2, \gamma_3) \mid E = h,\ F_1 = 1\}.$$

To parameterize this flow, we shall use the variables ω_1, γ_1 and γ_2 by expressing ω_2 and γ_3 in terms of the integrals (2.6):

$$(\dot\omega_1, \dot\gamma_1, \dot\gamma_2) = \mathcal{F}(\omega_1, \gamma_1, \gamma_2)^{1)}.$$

Choosing the plane $\gamma_1 = \text{const}$ as the secant of the three-dimensional flow $\mathcal{F}$, we obtain a two-dimensional Poincaré map[2)]

$$(\bar\gamma_2, \bar\omega_1) = \mathcal{P}(\gamma_2, \omega_1). \tag{4.1}$$

Since the variables γ_3 and ω_2 are defined in terms of the integrals repeatedly, the resulting map is many-leaved (the choice of the signs γ_3 and ω_2 defines a specific leaf). For definiteness, in what follows we shall choose a leaf corresponding to positive values of the variable ω_2.

On the constructed two-dimensional Poincaré map $\mathcal{P}$, the fixed points correspond to periodic orbits (cycles) in the initial system (2.5).

[1)] In this case ω_2 and γ_3 are easily expressed in terms of the energy and geometric integrals. Since the variables ω_1 and ω_2 appear in Eqs. (2.5) equivalently, we can write in a similar way the three-dimensional flow in the variables $(\omega_2, \gamma_1, \gamma_2)$.

[2)] For more on the procedure of constructing Poincaré maps for various problems of rigid body dynamics, see the book [32].

4.1. Reversibility and Involutions

The studies [13, 17, 31] show that the presence of reversibility and the number of involutions in the system considerably influence the type and complexity of the dynamics of nonholonomic systems. The papers [17, 31] are concerned with the motion of rigid bodies of different forms moving on the surface without slipping and spinning. In these papers it is shown that, depending on the geometrical and dynamical properties of the body, the system can have different numbers of involutions, which ultimately determines the type of chaotic dynamics in the system. The results of investigation of the Chaplygin top (a dynamically asymmetric ball with a displaced center of mass) are presented in [13]. In the case of an arbitrary displacement of the center of mass of this top the system is reversible under the only involution, and the top itself can execute a reversal (like a rattleback). Moreover, a strange attractor of figure-of-eight type was found in this case. The papers [6, 7] are concerned with the motion of a rattleback. In these papers it is also noted that the rattleback dynamics is also connected with involutions.

We now turn to analysis of reversibility in the system (2.5). In the general case (with any parameters) the system is reversible only under one involution

$$R_0 : \omega_1 \to -\omega_1, \quad \omega_2 \to -\omega_2, \quad t \to -t. \tag{4.2}$$

Remark. We recall that a system is said to be *reversible* under *involution* R if this system is invariant under R and the time reversal $t \to -t$, and the transformation $R \circ R$ is an identity transformation.

Due to this involution the phase portrait of the system (2.5) possesses the following properties:

- For each trajectory $\mathcal{F}(\gamma_1, \gamma_2, \omega_1)$ there exists a symmetric (relative to $Fix(R_0) = \{\omega_1 = \omega_2 = 0\}$) trajectory $\mathcal{F}^{-1}(R_0(\gamma_1, \gamma_2, \omega_1))$ which is in involution with the initial one.
- If the set A is an attractor, then the set $R_0(A)$ is attracting for the flow in reverse time $\mathcal{F}^{-1}$, i.e., it is a repeller.

In Section 5 it will be shown that the properties described above give rise to a reversal in the system (2.5) and that this reversal can be of the same type as for rattlebacks.

Consider the Suslov top whose center of mass is displaced only along the axis Ox_3, i.e., $\boldsymbol{b} = (0, 0, b_3)$. In this case, depending on the tensor of inertia $\mathbf{I}$, additional involutions may appear in the system (2.5). A complete list of these involutions is presented in the table below:

Table 1. Additional involutions of the system (2.5) for $\boldsymbol{b} = (0, 0, b_3)$.

	$I_{13} = 0$, $I_{23} = 0$	$I_{13} = 0$, $I_{23} \neq 0$	$I_{13} \neq 0$, $I_{23} = 0$	$I_{13} \neq 0$, $I_{23} \neq 0$
R_1: $\omega_1 \to -\omega_1$, $\gamma_1 \to -\gamma_1$, $t \to -t$	+	+	−	−
R_2: $\omega_2 \to -\omega_2$, $\gamma_2 \to -\gamma_2$, $t \to -t$	+	−	+	−

In order to carry over the above-mentioned involutions to the Poincaré map (4.1), we have to define as a secant a manifold that is invariant under an involution. Therefore, the most suitable secant for the system (2.5) is the hyperplane $\gamma_1 = 0$. We note that on the Poincaré map (4.1) we work with a leaf that corresponds to a specific positive value of the variable ω_2, and hence some involutions (for example, R_0 and R_2) cannot be carried over.

Thus, under the choice of the secant $\gamma_1 = 0$ and the additional condition $I_{13} = 0$ the constructed Poincaré map (4.1) can possess the only involution

$$r_1 : \omega_1 \to -\omega_1, \tag{4.3}$$

whose set of fixed points forms the straight line

$$Fix(r_1) = \{\omega_1 = 0\}.$$

In Section 6 we will need the straight line $Fix(r_1)$ for the investigation and classification of chaotic dynamics. For convenience, we introduce the following definitions. We use the term *reversible attractor* for a limiting set formed by iterations (on the Poincaré map) of the line $\omega_1 = 0$ in direct time and the term *reversible repeller* for a limiting set consisting of iterations of this line in reverse time. By the Poincaré reversibility theorem [34], in the case of existence of a smooth invariant measure in the system, the reversible attractor and the reversible repeller are undistinguishable. Otherwise these sets are distinguishable, but symmetric to each other relative to $Fix(r_1) = \{\omega_1 = 0\}$. In Section 6 we shall use the degree of such distinguishability for the classification of chaotic regimes.

Figure 3 shows phase portraits of the system (2.5) with different parameters. For the Suslov top for which $I_{13} = 0$, the Poincaré map is involutive relative to the straight line $\omega_1 = 0$ (see Fig. 3a).

In the general case, the Poincaré map (4.1) admits no involutions and exhibits visible crowdings of points (practically black regions) corresponding to simple attractors, which are fixed and periodic points (see Fig. 3b). As is well known, the existence of any attractors is an obstacle to the existence of a smooth invariant measure. Moreover, the presence of a chaotic layer is indicative of the absence of the additional first integral F_2.

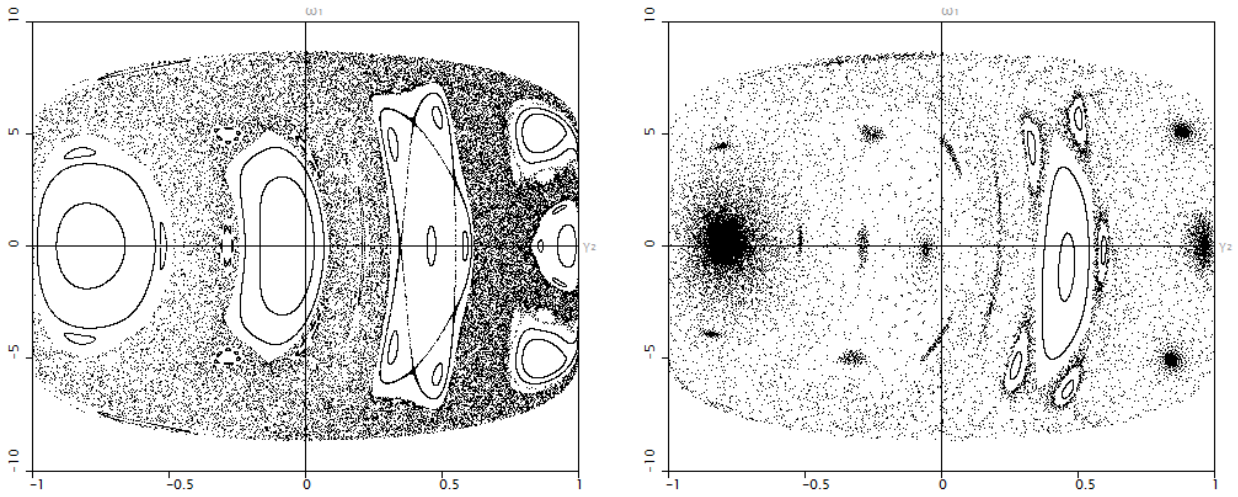

a) $I_{13} = 0$ b) $I_{13} = 0.1$

Fig. 3. Phase portrait on the Poincaré map (4.1). All parameters, except for I_{13}, are chosen as follows: $E = 50, I_1 = 4, I_2 = 3, I_{23} = 0, \boldsymbol{b} = (0, 0, 100)$. a) Due to the presence of the involution r_1 the phase portrait on the Poincaré map looks symmetric relative to the horizontal axis. b) When $I_{13} \neq 0$, the involution r_1 disappears, and the phase portrait on the Poincaré map becomes nonsymmetric. Moreover, on the Poincaré map one can see crowdings of trajectories near asymptotically stable points of different periods.

5. REVERSAL AND FIXED POINTS

In this section we present results on the equilibria of the system (2.5) for an unbalanced Suslov top ($\boldsymbol{b} \neq 0$) whose mass distribution is given by the nondiagonal tensor of inertia ($I_{13}^2 + I_{23}^2 \neq 0$).

5.1. Fixed Points of the Reduced System

On the fixed level set of the geometrical integral ($F_1 = 1$), for $\boldsymbol{b} \neq 0$ and $I_{13}^2 + I_{23}^2 \neq 0$ the system (2.6) exhibits three families of equilibrium points:

1. Pair of isolated equilibrium points

$$\Omega_1 = \left\{ \omega_1 = 0, \omega_2 = 0, \gamma_1 = \pm\frac{b_1}{\sqrt{\boldsymbol{b}^2}}, \gamma_2 = \pm\frac{b_3}{\sqrt{\boldsymbol{b}^2}}, \gamma_3 = \pm\frac{b_3}{\sqrt{\boldsymbol{b}^2}} \right\}.$$

2. One-parameter family of equilibrium points of the form:

$$\Omega_2 = \left\{ \omega_1 = \sin\varphi\sqrt{\frac{b_3}{A}}, \omega_2 = \cos\varphi\sqrt{\frac{b_3}{A}}, \gamma_1 = \sin\varphi, \gamma_2 = \cos\varphi, \gamma_3 = 0 \right\},$$

3. One-parameter family of equilibrium points of the form:

$$\Omega_3 = \left\{ \omega_1 = -\sin\varphi\sqrt{\frac{b_3}{A}}, \omega_2 = -\cos\varphi\sqrt{\frac{b_3}{A}}, \gamma_1 = \sin\varphi, \gamma_2 = \cos\varphi, \gamma_3 = 0 \right\}.$$

The variable A and the angle φ (depending on the sign of parameter b_3) for the families Ω_2 and Ω_3 are expressed as follows:

$$A = I_{13}\sin\varphi + I_{23}\cos\varphi,$$
$$\varphi \in (\widetilde{\varphi}, \pi + \widetilde{\varphi}) \text{ if } \quad b_3 > 0,$$
$$\varphi \in (\pi + \widetilde{\varphi}, 2\pi + \widetilde{\varphi}) \text{ if } \quad b_3 < 0,$$
$$\widetilde{\varphi} = -\arctan\frac{I_{23}}{I_{13}}.$$

A pair of isolated equilibrium points of the family Ω_1 lies on the fixed level set of the energy integral $h = \pm b_3$ and has a characteristic polynomial of the form

$$P(\lambda) = \lambda\left(-\lambda^4 \pm \left(\frac{b_1^2 + b_3^2}{I_{22}\sqrt{\boldsymbol{b}^2}} + \frac{b_2^2 + b_3^2}{I_{22}\sqrt{\boldsymbol{b}^2}}\right)\lambda^2 - \frac{b_3^2}{I_{11}I_{22}}\right). \tag{5.1}$$

We note that at isolated equilibrium points the energy integral $E = h$ and the geometric integral $F_1 = 1$ are dependent, therefore the characteristic polynomial has only one zero root. Analysis of the other roots of Eq. (5.1) shows that one of the equilibrium points is a center and the other is a conservative saddle.

Consider in more detail the second and the third families of fixed points. Substituting the equilibrium from Ω_2 (or Ω_3) into (2.6), we obtain an equation relating φ to the level set of the energy integral $E = h$:

$$h(\varphi) = \frac{b_3}{2A}(I_{11}\sin^2\varphi + I_{22}\cos^2\varphi) + b_1\sin\varphi + b_2\cos\varphi. \tag{5.2}$$

A typical dependence $h(\varphi)$ in the case $b_3 > 0$ is shown in Fig. 4.

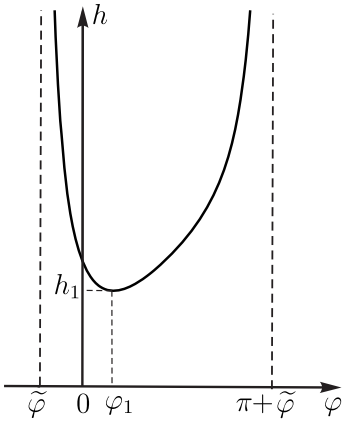

Fig. 4. Dependence $h(\varphi)$.

Thus, at small values of the parameter of energy $h < h_1$ the system (2.5) exhibits no equilibria from the families Ω_2 and Ω_3; when $h = h_1$, 2 equilibria appear, and when $h > h_1$, there are 4 of them.

The characteristic equation for the second family Ω_2 of equilibria of the linearized system is written as

$$\begin{gathered} P(\lambda) = \lambda^2(p_1\lambda^3 + p_2\lambda^2 + p_3\lambda + p_4), \\ p_1 = -I_{11}I_{22}A, \quad p_2 = (I_{11}I_{23}\sin\varphi - I_{22}I_{13}\cos\varphi)\sqrt{Ab_3}, \\ p_3 = A(I_{11}b_1\sin\varphi + I_{22}b_2\cos\varphi) - b_3(I_{11}I_{22} + 2A^2), \\ p_4 = 2A\sqrt{Ab_3}(b_1\cos\varphi - b_2\sin\varphi) \\ + (I_{11} - I_{22})\sqrt{Ab_3}\sin\varphi\cos\varphi + \sqrt{Ab_3}(I_{11}I_{23}\sin\varphi - I_{22}I_{13}\cos\varphi). \end{gathered} \tag{5.3}$$

Remark. For $I_{13}^2 + I_{23}^2 \neq 0$ the trace of the linearization matrix is equal to $-\frac{p_2}{p_1} \neq 0$, which is indicative of the absence of a smooth invariant measure in the system (2.6) in the case considered [35].

Remark. We note that the third family of equilibrium points is in involution R_0 with the second family. Hence, if the equilibrium point $O_1 \in \Omega_2$ possesses the eigenvalues $\lambda_1, \ldots, \lambda_5$, then $O_2 = R_0(O_1)$ belongs to the family Ω_3 and has the eigenvalues $-\lambda_1, \ldots, -\lambda_5$. Thus, in what follows we shall investigate the equilibria belonging only to the family Ω_2.

In the general case, on each level set of the energy integral $E > h_1$ the family Ω_2 contains 2 equilibrium points, of which each has 3 nonzero eigenvalues $(\lambda_1^{(i)}, \lambda_2^{(i)}, \lambda_3^{(i)}), i = 1, 2$.

We note that the coefficients of the characteristic equation (5.3) depend not only on the system parameters, but also on the angle φ, which in its turn is expressed in terms of the energy integral from Eq. (5.2). Thus, it is difficult to perform stability analysis of the equilibria analytically.

For a numerical stability analysis of equilibrium points belonging to the family Ω_2 we construct a diagram of stability of equilibrium points on the plane of parameters (I_{23}, E) by fixing the other parameters by the following values:

$$I_1 = 4, I_2 = 2, I_{13} = 1.5, b_1 = 0, b_2 = 0, b_3 = 100. \tag{5.4}$$

For the above parameters the characteristic equation always possesses one real root (for definiteness λ_1) and a pair of complex conjugate roots.

To construct the stability diagram, we divide the parameter plane (I_{23}, E) into 200×200 points, and color each of the points, depending on the number of equilibrium points and their types, in a particular color in accordance with the following rules:

- there exist no equilibrium points — gray;
- 2 equilibrium points for which $\lambda_1^{(1)} > 0, \mathrm{Re}(\lambda_{2,3}^{(1)}) < 0$ and $\lambda_1^{(2)} < 0, \mathrm{Re}(\lambda_{2,3}^{(2)}) < 0$ — green;
- 2 equilibrium points for which $\lambda_1^{(1)} < 0, \mathrm{Re}(\lambda_{2,3}^{(1)}) > 0$ and $\lambda_1^{(2)} > 0, \mathrm{Re}(\lambda_{2,3}^{(2)}) > 0$ — blue.

We comment on the stability diagram plotted in Fig. 5. For small energies ($E < h_1$) there are no equilibrium points in the system. When a critical level of energy $E = h_1$ is attained, a saddle-node bifurcation occurs in the system, resulting in the birth of a saddle-node equilibrium, which breaks up, with further increase of energy, into a stable node ($\lambda_1^{(1)} < 0, \mathrm{Re}(\lambda_{2,3}^{(1)}) < 0$) and a saddle ($\lambda_1^{(2)} > 0, \mathrm{Re}(\lambda_{2,3}^{(2)}) < 0$).

Further, as the energy increases to the value $E = h_2$, the saddle equilibrium undergoes an Andronov – Hopf bifurcation and (when $E > h_2$) becomes completely unstable ($\lambda_1^{(2)} > 0, \mathrm{Re}(\lambda_{2,3}^{(2)}) > 0$). We note that the Andronov – Hopf bifurcation can be of two types in this case (for a detailed description see Section 6).

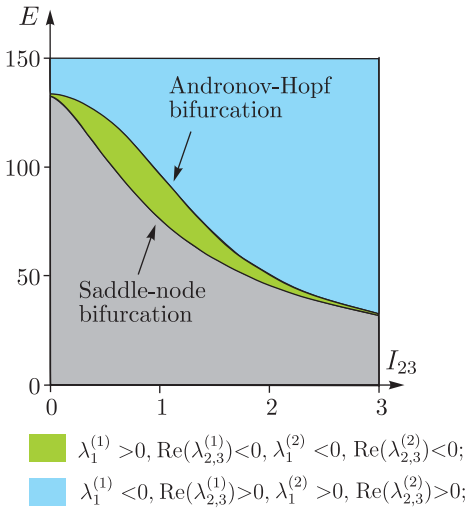

Fig. 5. Diagram showing the stability of equilibrium points from the family Ω_2 for the parameters (5.4).

5.2. The Motion of a Rigid Body in Absolute Space at Fixed Points

Consider the absolute motions of the Suslov top on each of the three families of equilibrium points.

At isolated equilibrium points of the family Ω_1 the rigid body remains fixed in the coordinate system $Oxyz$. For an equilibrium point of saddle type, the center of mass of the Suslov top lies on the axis Oz below the fixed point, and for an equilibrium point of center type it lies above the fixed point.

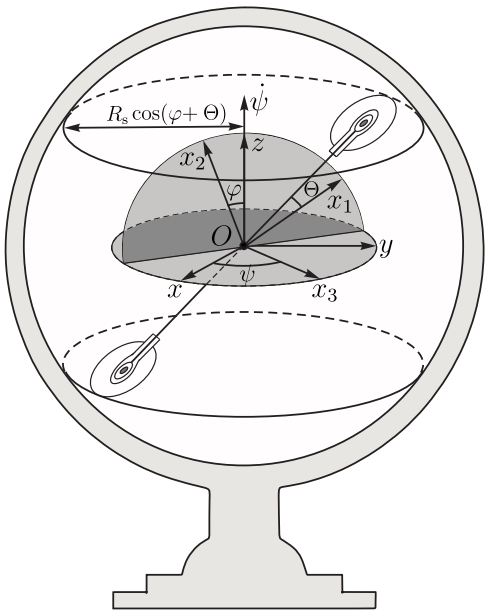

Fig. 6. The motion of a rigid body at equilibrium points belonging to the families Ω_2 and Ω_3 of the system (2.5)

At equilibrium points belonging to the families Ω_2 and Ω_3, the vectors $\boldsymbol{\omega}$ and $\boldsymbol{\gamma}$ are collinear. Therefore, the Suslov top rotates with constant velocity about the axis Oz. Since $\gamma_3 = 0$ on the families under consideration, the axis Ox_3 is always in the plane Oxy, and the parameter φ defines

the angle between Oz and Ox_2. The equation of precession (2.7) takes the form

$$\dot{\psi} = \pm\sqrt{\frac{b_3}{A}}.$$

When the Suslov top rotates, the point of contact of the wheels with the (fixed) sphere moves in a circle with the center $(0, 0, \pm R_s \sin(\varphi + \Theta))$, where R_s is the radius of the sphere and Θ is the angle of rotation of the axis connecting the wheels relative to the axis Ox_1 (see Fig. 6).

Remark. We recall that the orientation of the axes Ox_1 and Ox_2 and hence the angle Θ have been chosen in such a way that one of the components of the tensor of inertia (I_{12}) vanishes.

5.3. Reversal

Depending on the number of stable and unstable equilibria in the system (2.5), various types of motions of the Suslov top in absolute space are possible.

For the choice of parameters corresponding to the narrow region (colored green) in Fig. 5, the system has, along with a pair of saddle equlibria, a stable O^+ and a completely unstable O^- equilibrium, which are in involution R_0, i.e., $O^+ = R_0(O^-)$. Trajectories started from a neighborhood of the completely unstable equilibrium O^- can pass to a neighborhood of the stable equilibrium O^+. As a result of this transition, the axis of rotation of the top (Ox_3) turns over (see Fig. 7). In absolute space, this process corresponds to a reversal of the direction of the top's rotation about the fixed vertical axis. As mentioned previously, this type of reversal was first discovered in the course of investigating the rattleback [4, 5].

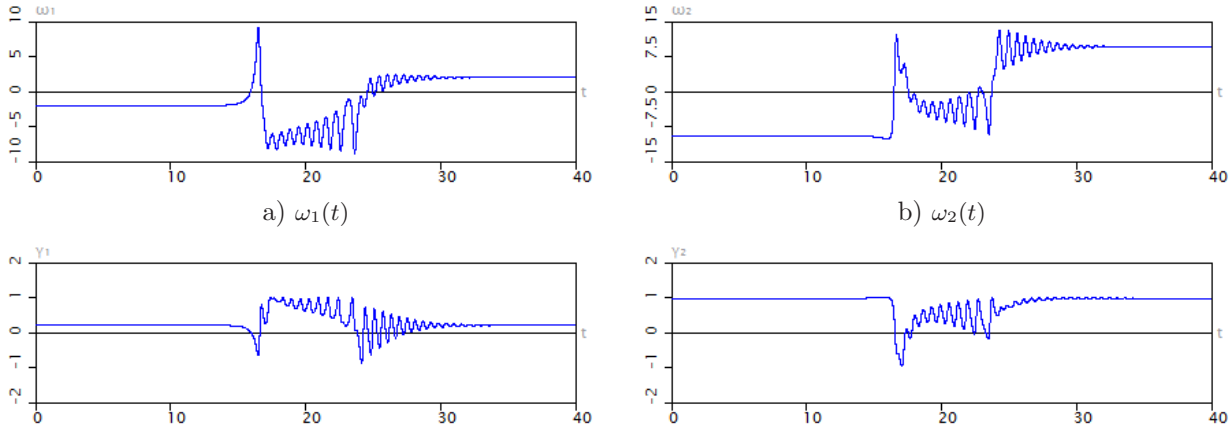

Fig. 7. Time dependence of the phase variables at the start of the trajectory from the neighborhood of an unstable equilibrium for $E = 100, I_1 = 4, I_2 = 2, I_{13} = 1.5, I_{23} = 0.75, b_1 = 0, b_2 = 0, b_3 = 100$.

The large region colored blue in Fig. 5 corresponds to parameter values at which the system (2.5) has a pair of stable equilibria and a pair of completely unstable equilibria. As numerical experiments show, the trajectories started near one of the unstable equilibria ($\widetilde{O}^-$) can pass in this case to a neighborhood of the stable equilibrium ($\widetilde{O}^+$), which (as opposed to the previous case) is not in involution R_0 with the initial one. During such a transition the axis of rotation Ox_3 rotates through angle $\Delta\varphi$ (see Fig. 8):

$$\Delta\varphi = \arctan\left(\frac{\widetilde{\gamma_1}^{(+)}}{\widetilde{\gamma_2}^{(+)}}\right) - \arctan\left(\frac{\widetilde{\gamma_1}^{(-)}}{\widetilde{\gamma_2}^{(-)}}\right).$$

In this case, the body changes orientation in absolute space. As a result, the angle between the axes Ox_2 and Oz changes by $\Delta\varphi$.

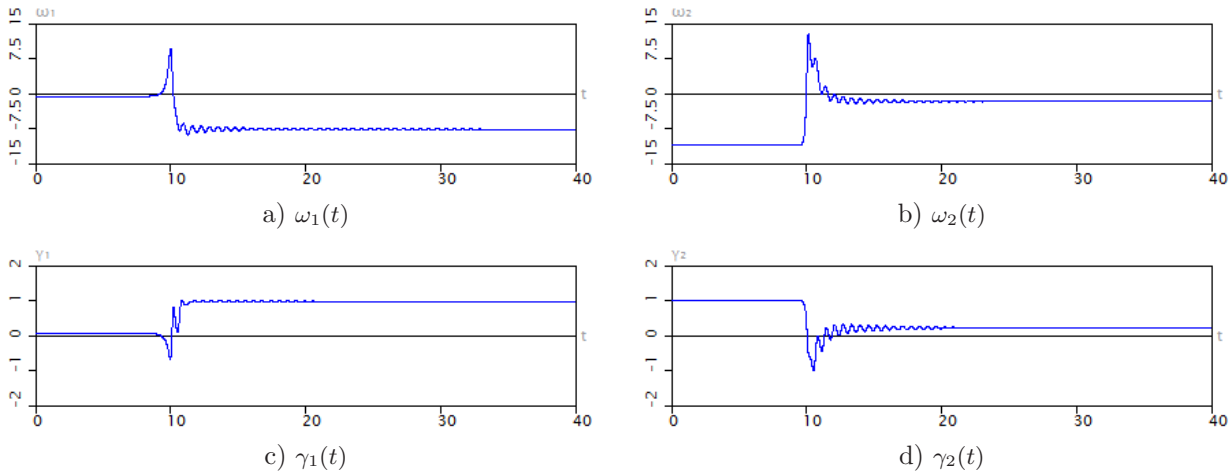

a) $\omega_1(t)$ b) $\omega_2(t)$

c) $\gamma_1(t)$ d) $\gamma_2(t)$

Fig. 8. Time dependence of the phase variables at the start of the trajectory from the neighborhood of an unstable equilibrium for $E = 120, I_1 = 4, I_2 = 2, I_{13} = 1.5, I_{23} = 0.75, b_1 = 0, b_2 = 0, b_3 = 100$.

It is evident from Fig. 4 that $\Delta\varphi \to \pm\pi$ as $E \to \infty$. That is, at very large energies the Suslov top started in a neighborhood of an unstable equilibrium turns over and continues a stable rotation about the overturned axis. Previously such an effect was observed for the Thompson top (tippe-top) [14] in a natural experiment and in the nonholonomic model of rolling of a dynamically asymmetric ellipsoid of revolution [15].

6. CHAOTIC DYNAMICS

In this section we present numerical results on the chaotic dynamics in the nonholonomic Suslov model and show that the system under consideration exhibits complex chaotic behavior whose type essentially depends on the system parameters and hence on the number of involutions.

We shall classify various limiting (including chaotic) regimes by analyzing the charts of Lyapunov exponents on the parameter plane (I_{23}, E) by fixing the other system parameters.

We describe the scheme of constructing the charts of Lyapunov exponents[3)]. We divide the parameter plane (I_{23}, E) into 400×400 nodes and start from each node a trajectory on the Poincaré map (4.1) with some initial conditions (γ_2, ω_1). To preclude a transient process, the system was integrated for $T = 4 \cdot 10^4$ time units, and then the Lyapunov exponents were estimated on the interval $T = 10^4$ by the Benettin method [36]. Depending on the values of λ_1, λ_2 and λ_3, we color the corresponding node in the chart in a particular color.

We note that the system (2.5) possesses three essential (nonzero) exponents $\lambda_1 \geqslant \lambda_2 \geqslant \lambda_3 > 0$. To exclude from consideration two zero exponents, which correspond to the integrals (2.6), we apply the procedure of normalization of phase variables to the level sets of the integrals [37].

Further we shall consider 2 fundamentally different cases:

- $I_{13} = 0$ — the system (2.5) is reversible under two involutions: R_0 and R_1;
- $I_{13} \neq 0$ — the system (2.5) is reversible under the only involution R_0.

[3)] For more on the methods of constructing the charts of Lyapunov exponents, see, for example, in [13, 37], where such charts are constructed for nonholonomic systems describing the rolling motion of a rattleback and the Chaplygin top, respectively. However, in this paper we have slightly modified the procedure of classification of chaotic regimes.

6.1. Chaotic Dynamics for $I_{13} = 0$

In the case considered, the Poincaré map (4.1) is symmetric relative to the straight line $Fix(R_1) = \{\omega_1 = 0\}$. To construct a chart of Lyapunov exponents, we fix the system parameters by the following values:

$$I_{13} = 0, \quad I_1 = 3, I_2 = 4, b_1 = 0, b_2 = 0, b_3 = 100, \tag{6.1}$$

and as the initial point for each node of the chart we use a point with coordinates $(\gamma_2, \omega_1) = (0.9, 0.1)$. We give some explanations on the regimes depicted in the chart (see Fig. 9). Among the regular regimes ($\lambda_1 \leqslant 0$) in the chart of Lyapunov exponents we distinguish:

- $\lambda_1 < 0$ — equilibrium;
- $\lambda_1 = 0 \quad \lambda_1 + \lambda_2 + \lambda_3 < 0$ — cycle (a periodic or fixed point on the map (4.1));
- $\lambda_1 = 0, \quad \lambda_1 + \lambda_2 + \lambda_3 = 0$ — elliptic orbit (invariant curves around an elliptic point or the elliptic point itself).

In addition to regular limiting regimes in the chart of Lyapunov exponents, we shall also classify various chaotic ($\lambda_1 > 0$) regimes. We note that the case $\lambda_1 > 0$, $\lambda_1 + \lambda_2 + \lambda_3 = 0$ corresponds to conservative chaos (see Fig. 9 on the left), in which the phase volume (invariant measure) is conserved. In this case the reversible attractor and the reversible repeller are indistinguishable.

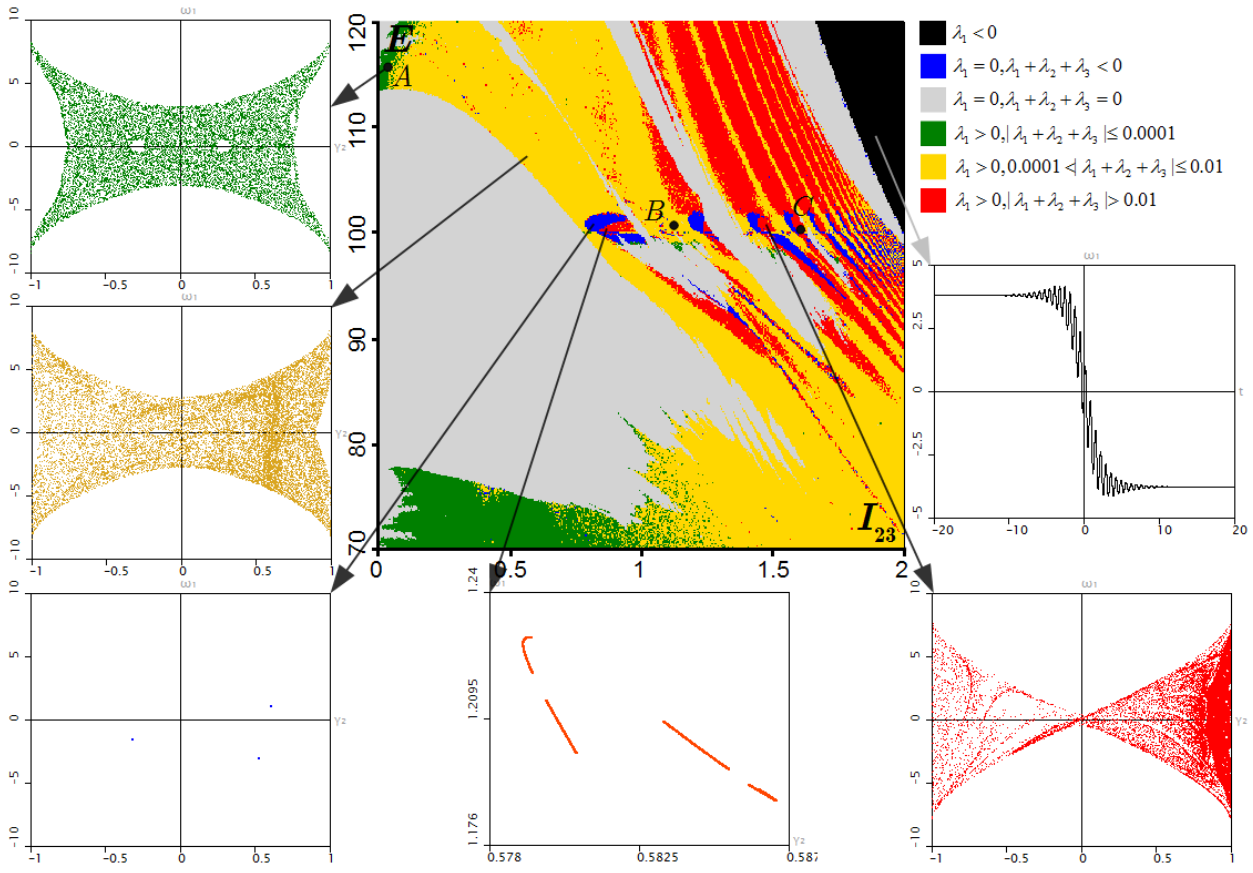

Fig. 9. Chart of Lyapunov exponents and the typical phase portraits for different values of the parameters I_{23} and E. The other parameters have been chosen according to (6.1).

If the system (2.5) does not possess a smooth invariant measure, then the reversible attractor and the reversible repeller become distinguishable. Following the paper [38], which has opened new prospects for the study of reversible systems, we shall characterize the degree of such

distinguishability by time-average divergence, i. e., by the sum of Lyapunov exponents (coexistence of dissipative and conservative effects in them is systematically discussed in the review [39]). Depending on this value, we classify the chaotic regimes as follows:

- $\lambda_1 > 0, \quad |\lambda_1 + \lambda_2 + \lambda_3| \leqslant 0.0001$. The case considered is close to a conservative one. The reversible attractor and the reversible repeller are practically indistinguishable (see Fig. 10).
- $\lambda_1 > 0, \quad 0.0001 < |\lambda_1 + \lambda_2 + \lambda_3| \leqslant 0.01$. In this case the reversible attractor and the reversible repeller, although they have a large common part, are distinguishable nevertheless (see Fig. 11). As shown in [17, 31] by constructing involutive networks, along with elliptic points (existing due to reversibility), the stochastic layer also has log-period foci whose boundary of attraction has a very small neighborhood. In this case, the behavior of the system may be said to be pseudoconservative.
- $\lambda_1 > 0, \quad 0.01 < |\lambda_1 + \lambda_2 + \lambda_3|$. The reversible attractor strongly differs from the reversible repeller, although it is symmetric to it (see Fig. 12). In this case, chaotic dynamics are associated with strange attractors.

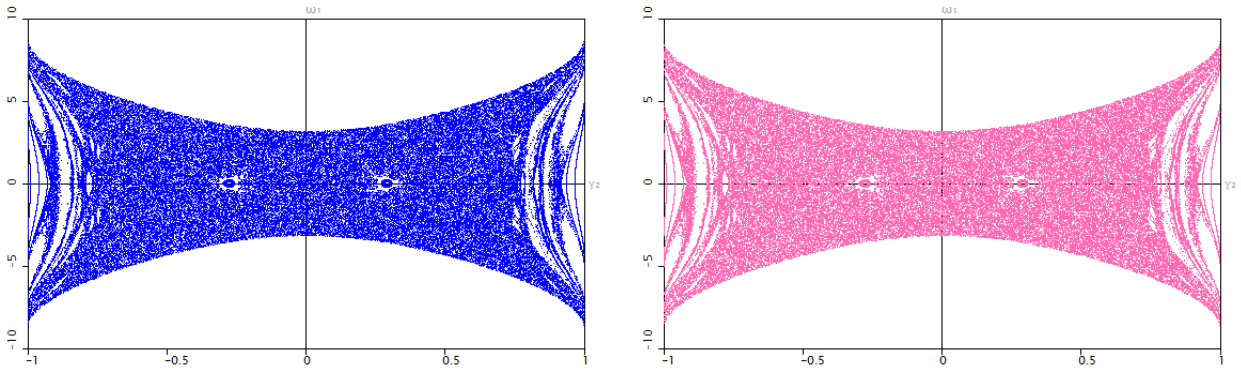

a) b)

Fig. 10. Phase portraits on the Poincaré map for the parameters (6.1), $I_{23} = 0.015, E = 115.125$ (point A in the chart of Lyapunov exponents (see Fig. 9)). (a) the reversible attractor and (b) the reversible repeller are practically indistinguishable.

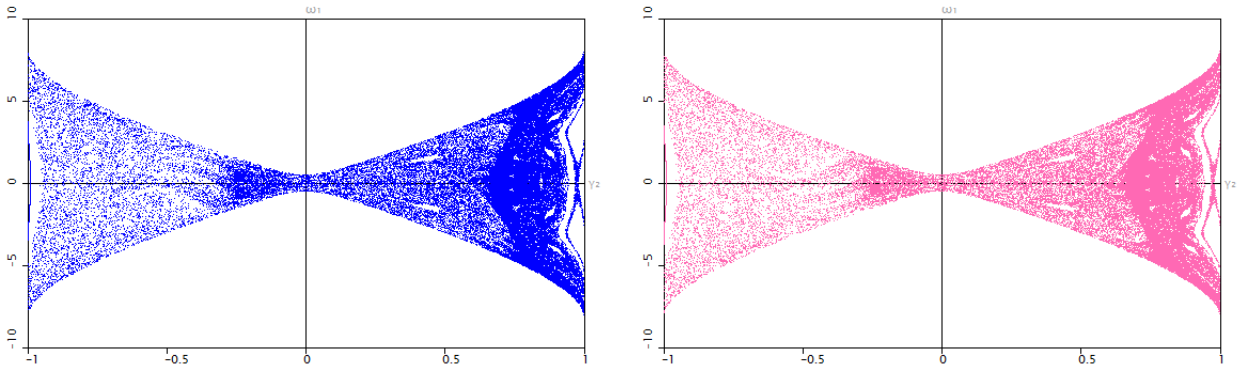

a) b)

Fig. 11. Phase portraits on the Poincaré map for the parameters (6.1), $I_{23} = 1.5, E = 100$ (point B in the chart of Lyapunov exponents (see Fig. 9)). The reversible attractor and the reversible repeller have a large common part, but are distinguishable nevertheless.

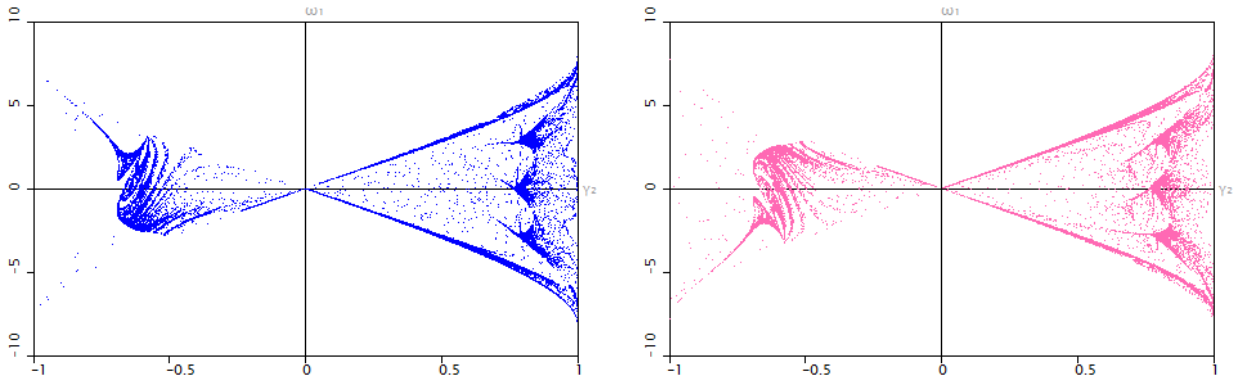

a) strange attractor b) strange repeller

Fig. 12. The strange attractor and the strange repeller on the Poincaré map (4.1) for $I_{23} = 1.5895$ and $E = 100$.

6.2. Chaotic Dynamics for $I_{13} \neq 0$

In this section, in constructing a chart of Lyapunov exponents, we shall use system parameters given in accordance with (5.4), in order to compare the chart of Lyapunov exponents with the stability diagram presented in Fig. 5. In each node of the chart, as the initial point we define a point with coordinates $(\gamma_2, \omega_1) = (0.999, 0)$. In the chart of Lyapunov exponents we keep to the classification of regimes given in Section 6.1. We only emphasize that in the case at hand (since the Poincaré map possesses no involutions) the notions *reversible attractor* and *reversible repeller* are undefined. Now the sum of Lyapunov exponents characterizes the degree of compression of the phase volume along the trajectory. For convenience, we present the stability diagram plotted earlier and the chart of Lyapunov exponents in one figure (Fig. 13).

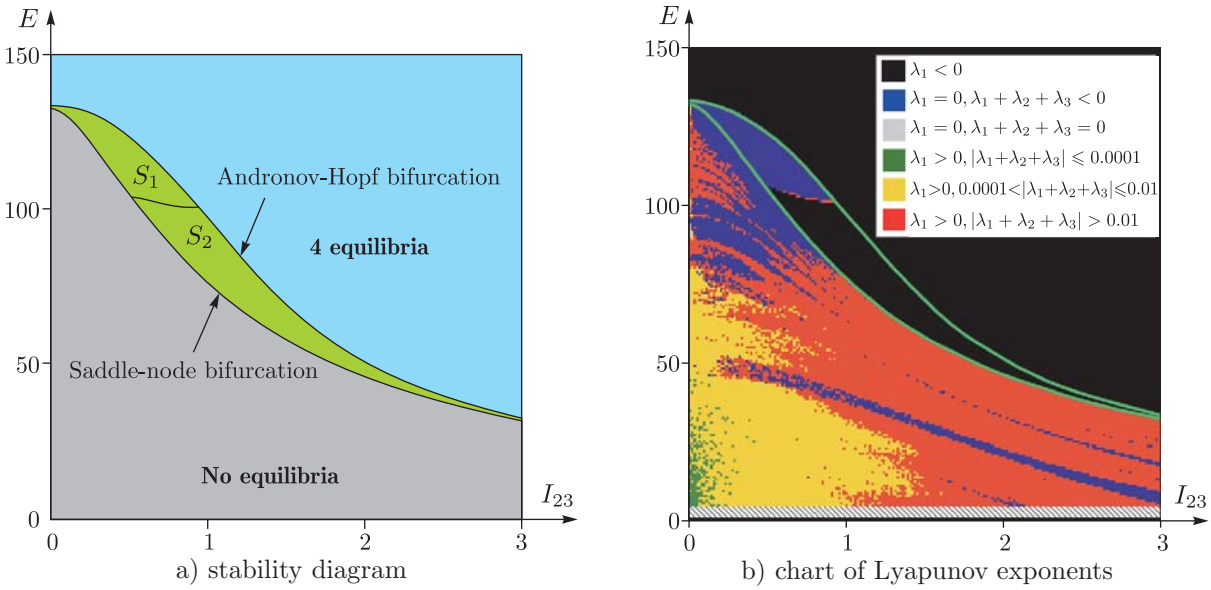

a) stability diagram b) chart of Lyapunov exponents

Fig. 13. Stability diagram and the chart of Lyapunov exponents for the parameters (5.4)

Consider in more detail the parameter region (denoted by $\boldsymbol{S}$ and colored green) in the chart presented in the figure. As is shown in Section 5, in this region the system (2.5) possesses a pair of saddle $(\lambda_1^{(1)} > 0, \mathrm{Re}(\lambda_{2,3}^{(1)}) > 0$ and $\lambda_1^{(4)} < 0, \mathrm{Re}(\lambda_{2,3}^{(4)}) > 0)$, stable $(\lambda_1^{(2)} < 0, \mathrm{Re}(\lambda_{2,3}^{(2)}) < 0)$ and unstable $(\lambda_1^{(3)} > 0, \mathrm{Re}(\lambda_{2,3}^{(3)}) > 0)$ equilibria (see Fig. 14). The lower boundary of this region is

formed by parameters giving rise to a pair of saddle-node bifurcations in the system, and the upper boundary is formed by parameters giving rise to a pair of Andronov – Hopf bifurcations. However, as shown in Fig. 13b, the Andronov – Hopf bifurcations qualitatively differ for the upper part ($\boldsymbol{S}_1$) and the lower part ($\boldsymbol{S}_2$) of the region $\boldsymbol{S}$. In particular, in the region $\boldsymbol{S}_1$ we have detected, along with the equilibria, a stable cycle with the multipliers $|\mu_1| < 1$ and $|\mu_2| < 1$. On the upper boundary of the region $\boldsymbol{S}_1$ this stable cycle merges with the saddle equilibrium $(\lambda_1^{(4)} < 0, \mathrm{Re}(\lambda_{2,3}^{(4)}) > 0)$; as a result, this equilibrium becomes stable $(\lambda_1^{(4)} < 0, \mathrm{Re}(\lambda_{2,3}^{(4)}) < 0)$ (see Fig. 14 a)[4].

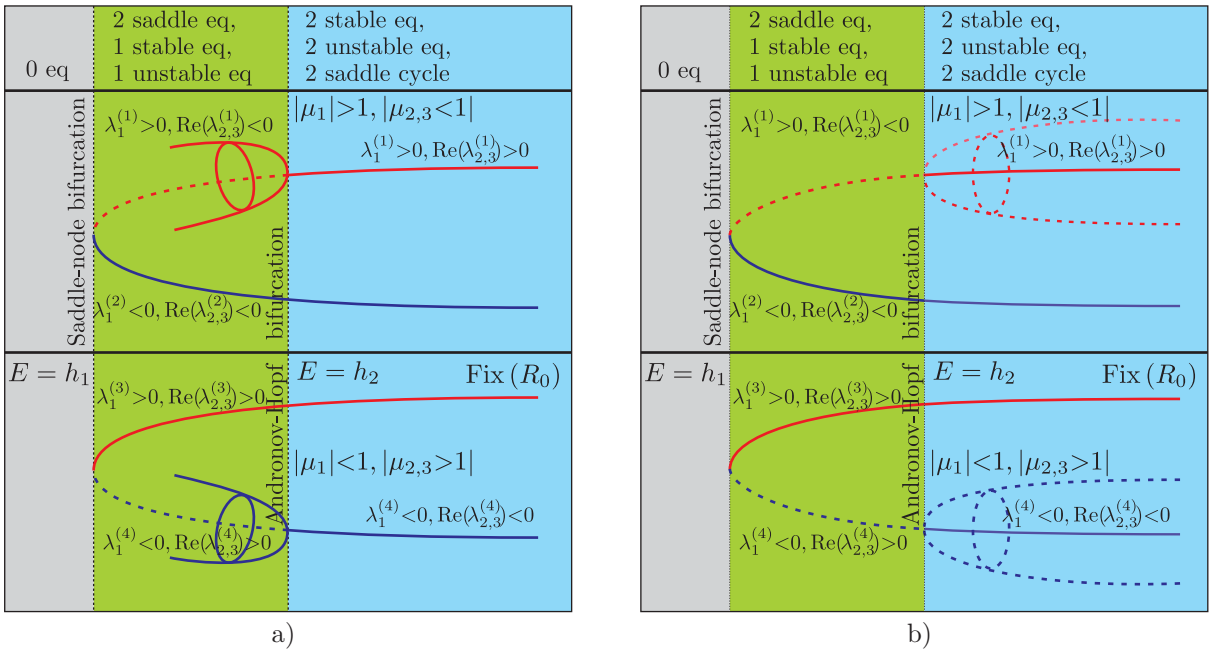

Fig. 14. Bifurcation diagrams of equilibria belonging to the families Ω_2 and Ω_3; a) — for the parameter region $\boldsymbol{S}_1$, b) — for the parameter region $\boldsymbol{S}_2$.

No stable cycle was observed in the region $\boldsymbol{S}_2$. However, we found a saddle cycle slightly above the upper boundary of this region. Thus, on the upper boundary of the region $\boldsymbol{S}_2$ the saddle cycle with the multipliers $|\mu_1| > 1, |\mu_2| < 1$ separates from the saddle point as a result of a subcritical Andronov – Hopf bifurcation, and the saddle point becomes completely unstable $(\lambda_1^{(1)} > 0, \mathrm{Re}(\lambda_{2,3}^{(1)}) > 0)$. For convenience, the bifurcations described above are presented in Fig. 14b.

Continuously varying the parameter E, we observe changes in the fixed point that corresponds to the stable cycle detected in the region $\boldsymbol{S}_1$, we detected a sequence of period doubling bifurcations, as a result of which a strange attractor of Feigenbaum type [18] is born from the fixed point (see Fig. 15). The detected attractor corresponds to the following Lyapunov exponents.

$$\Lambda_1 = 0.3978, \quad \Lambda_2 = -0.0002, \quad \Lambda_3 = -1.9277,$$

and the Kaplan – Yorke dimension of the attractor [37] is

$$D = 1 + \frac{\Lambda_1}{|\Lambda_3|} \approx 1.2063.$$

[4] Due to involution R_0 the second saddle equilibrium $(\lambda_1^{(1)} > 0, \mathrm{Re}(\lambda_{2,3}^{(1)}) < 0)$ undergoes an Andronov – Hopf bifurcation of the same type. After this equilibrium merges with a completely unstable cycle, it becomes unstable $(\lambda_1^{(1)} > 0, \mathrm{Re}(\lambda_{2,3}^{(1)}) > 0)$.

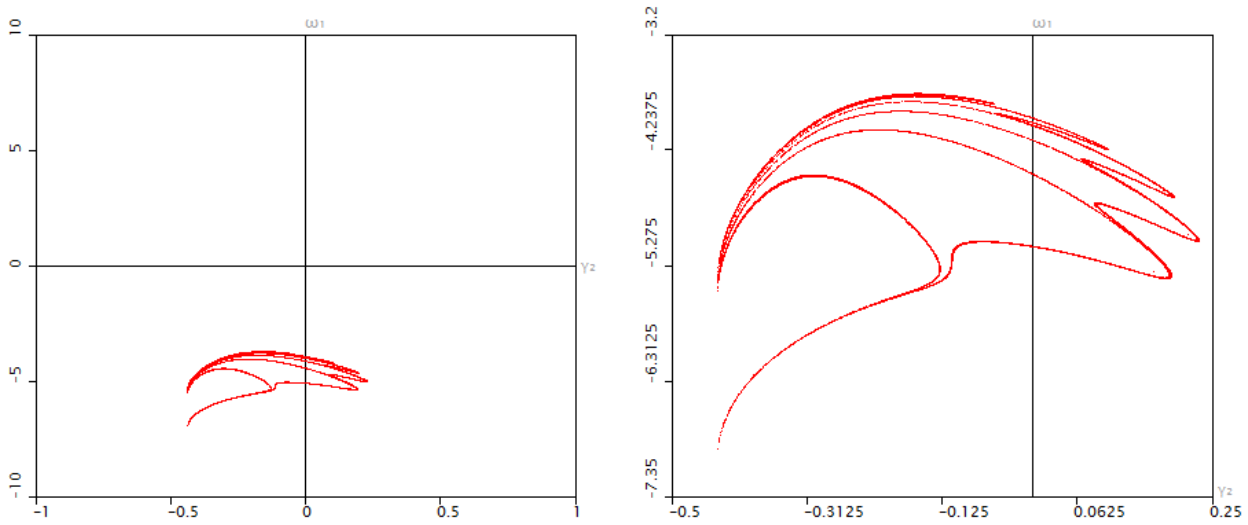

a) b)

Fig. 15. Strange attractor of Feigenbaum type detected at the boundary of regions $\boldsymbol{S}_1$ and $\boldsymbol{S}_2$ for the parameters (5.4) and $I_{23} = 0.675$, $E = 102.75$.

7. THE SUSLOV PROBLEM IN THE CASE OF AN INHOMOGENEOUS CONSTRAINT

Various generalizations (variations) of the Suslov problem are considered in [10, 33]. In this section we consider the case in which at the point of contact of the wheel with the fixed spherical shell there is a constant (time-independent) slipping s. This slipping can be interpreted as a deviation of the wheel as described by Y. Rocard. The deviation mechanics related to a deformation of the wheel is discussed in [41, 42].

The above condition leads to a nonholonomic constraint (inhomogeneous in velocities), which in the moving coordinate system $Ox_1x_2x_3$ has the form

$$\omega_3 = s, \quad s = \text{const}. \tag{7.1}$$

We note that theoretical research on inhomogeneous nonholonomic constraints has been started quite recently [29, 43–45]. Rewriting the system of Eqs. (2.3) and (2.4) in view of (7.1), we obtain equations of motion on $\mathcal{M}^5 = \{\omega_1, \omega_2, \gamma_1, \gamma_2, \gamma_3\}$ in the form

$$\begin{gathered} I_{11}\dot\omega_1 = -\omega_2(I_{13}\omega_1 + I_{23}\omega_2) + (I_2 - I_3)s\omega_2 + I_{23}s^2 + b_3\gamma_2 - b_2\gamma_3, \\ I_{22}\dot\omega_2 = \omega_1(I_{13}\omega_1 + I_{23}\omega_2) - (I_1 - I_3)s\omega_1 - I_{13}s^2 + b_1\gamma_3 - b_3\gamma_1, \\ \dot\gamma_1 = -\gamma_3\omega_2, \quad \dot\gamma_2 = \gamma_3\omega_1, \quad \dot\gamma_3 = \gamma_1\omega_2 - \gamma_2\omega_1. \end{gathered} \tag{7.2}$$

In the case $I_{13} = I_{23} = 0$ the system (7.2) possesses a standard invariant measure ($\rho = \text{const}$).

As is well known (see [29]), nonholonomic systems with constraints inhomogeneous in velocities are not energy-preserving. Therefore, in the general case the system (7.2) possesses only the geometric integral

$$F_1 = \boldsymbol{\gamma}^2 = 1.$$

However, there is a particular case in which it is possible to find a generalization of the energy integral — the *Jacobi integral*. In [29] it is shown that under the following restrictions to the parameters

$$I_{13} = I_{23} = 0, \quad I_{22} = I_{11}, \quad b_1 = b_2 = 0 \tag{7.3}$$

the system (7.2) possesses the Jacobi integral

$$H = \frac{I_{11}}{2}(\omega_1^2 + \omega_2^2) + b_3\gamma_3.$$

We note that conditions (7.3) coincide with the Kozlov case, in which there exists an additional integral F_2 for $s = 0$ (see Section 5). Moreover, it turns out that for $s \neq 0$ this integral admits the immediate generalization

$$F_2 = I_{11}(\omega_1\gamma_1 + \omega_2\gamma_2) + sI_{33}\gamma_3.$$

Thus, the system (7.2), when restricted to the parameters (7.3), is integrable by the Euler – Jacobi theorem.

However, in the general case the system (7.2) is nonintegrable. Figure 16 shows the phase portrait of the system (7.2) on the three-dimensional[5)] Poincaré map. We note that the Poincaré map (see Fig. 16) is not foliated into invariant surfaces; hence, in the general case the system (7.2) possesses neither of two additional integrals.

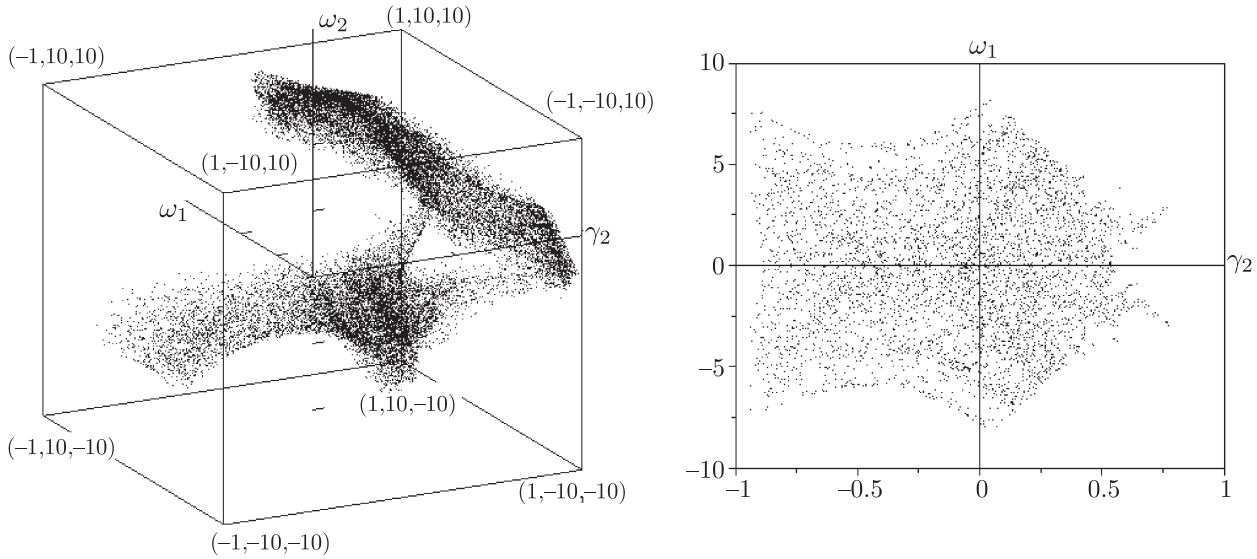

Fig. 16. Poincaré map and the section formed by its intersection with the plane $\omega_2 = 1$ for fixed $I_{11} = 3$, $I_{22} = 4$, $I_{33} = 5$, $I_{13} = I_{23} = 0$, $b_1 = b_2 = 0$, $b_3 = 100$, $s = 1$

Remark. If the center of mass of the rigid body is at the geometric center of the shell, i.e., $\boldsymbol{b} = 0$ and $I_{13}^2 + I_{23}^2 \neq 0$, a closed subsystem governing the evolution of ω_1 and ω_2 decouples in the system (7.2). This subsystem is considered in detail in [43], where cases of first integrals transcendental in velocities have been found.

ACKNOWLEDGMENTS

Sections 1, 3 and 7 were prepared by A. V. Borisov under the RSF grant No. 14-50-00005. Sections 2 and 5 were prepared by I. A. Bizyaev within the framework of the RFBR grants No. 15-38-20879 mol_a_ved and No. 15-08-09261-a. The work of A. O. Kazakov (Sections 4 and 6) was supported by RSF grant No. 15-12-20035.

REFERENCES

1. Borisov, A. V. and Mamaev, I. S., The Rolling Motion of a Rigid Body on a Plane and a Sphere: Hierarchy of Dynamics, *Regul. Chaotic Dyn.,* 2002, vol. 7, no. 2, pp. 177–200.
2. Borisov, A. V. and Mamaev, I. S., Conservation Laws, Hierarchy of Dynamics and Explicit Integration of Nonholonomic Systems, *Regul. Chaotic Dyn.,* 2008, vol. 13, no. 5, pp. 443–490.

[5)] In the case of the inhomogeneous nonholonomic constraint (7.1) the system (7.2) does not possess an energy integral, therefore the Poincaré map becomes three-dimensional.

3. Borisov, A. V., Kilin, A. A., and Mamaev, I. S., The Problem of Drift and Recurrence for the Rolling Chaplygin Ball, *Regul. Chaotic Dyn.,* 2013, vol. 18, no. 6, pp. 832–859.
4. Walker, G. T., On a Curious Dynamical Property of Celts, *Proc. Cambridge Phil. Soc.,* 1895, vol. 8, pt. 5, pp. 305–306.
5. Walker, J., The Amateur Scientist: The Mysterious ¡¡Rattleback¿¿: A Stone That Spins in One Direction and Then Reverses, *Sci. Am.,* 1979, vol. 241, pp. 172–184.
6. Borisov, A. V. and Mamaev, I. S., Strange Attractors in Rattleback Dynamics, *Physics–Uspekhi,* 2003, vol. 46, no. 4, pp. 393–403; see also: *Uspekhi Fiz. Nauk,* 2003, vol. 173, no. 4, pp. 408–418.
7. Gonchenko, A. S., Gonchenko, S. V., and Kazakov, A. O., Richness of Chaotic Dynamics in the Nonholonomic Model of Celtic Stone, *Regul. Chaotic Dyn.,* 2013, vol. 18, no. 5, pp. 521–538.
8. Suslov, G. K., *Theoretical Mechanics,* Moscow: Gostekhizdat, 1946 (Russian).
9. Vagner, V. V., A Geometric Interpretation of the Motion of Nonholonomic Dynamical Systems, *Tr. semin. po vectorn. i tenzorn. anal.,* 1941, no. 5, pp. 301–327 (Russian).
10. Borisov, A. V., Kilin, A. A., and Mamaev, I. S., Hamiltonicity and Integrability of the Suslov Problem, *Regul. Chaotic Dyn.,* 2011, vol. 16, nos. 1–2, pp. 104–116.
11. Fedorov, Yu. N., Maciejewski, A. J., and Przybylska, M., Suslov Problem: Integrability, Meromorphic and Hypergeometric Solutions, *Nonlinearity,* 2009, vol. 22, no. 9, pp. 2231–2259.
12. Kozlov, V. V., On the Theory of Integration of the Equations of Nonholonomic Mechanics, *Uspekhi Mekh.,* 1985, vol. 8, no. 3, pp. 85–107 (Russian).
13. Borisov, A. V., Kazakov, A. O., and Sataev, I. R., The Reversal and Chaotic Attractor in the Nonholonomic Model of Chaplygin's Top, *Regul. Chaotic Dyn.,* 2014, vol. 19, no. 6, pp. 718–733.
14. Kane, T. R. and Levinson, D. A., A Realistic Solution of the Symmetric Top Problem, *J. Appl. Mech.,* 1978, vol. 45, no. 4, pp. 903–909.
15. Borisov, A. V., Kilin, A. A., Mamaev, I. S., New Effects in Dynamics of Rattlebacks, *Dokl. Phys.,* 2006, vol. 51, no. 5, pp. 272–275; see also: *Dokl. Akad. Nauk,* 2006, vol. 408, no. 2, pp. 192–195.
16. Nordmark, A. and Essen, H., Systems with a Preferred Spin Direction, *Proc. R. Soc. London Ser. A*, 1999, vol. 455, no. 1983, pp. 933–941.
17. Kazakov, A. O., Strange Attractors and Mixed Dynamics in the Problem of an Unbalanced Rubber Ball Rolling on a Plane, *Regul. Chaotic Dyn.,* 2013, vol. 18, no. 5, pp. 508–520.
18. Feigenbaum, M. J., Universal Behavior in Nonlinear Systems, *Phys. D,* 1983, vol. 7, nos. 1–3, pp. 16–39.
19. Bolsinov, A. V., Borisov, A. V., and Mamaev, I. S., Topology and Stability of Integrable Systems, *Russian Math. Surveys,* 2010, vol. 65, no. 2, pp. 259–317; see also: *Uspekhi Mat. Nauk,* 2010, vol. 65, no. 2(392), pp. 71–132.
20. Kozlova, Z. P., The Suslov Problem, *Izv. Akad. Nauk SSSR. Mekh. Tverd. Tela,* 1989, no. 1, pp. 13–16 (Russian).
21. Kozlov, V. V., The Phenomenon of Reversal in the Euler – Poincaré – Suslov Nonholonomic Systems, *Preprint,* arXiv:1509.01089 (2015).
22. Kharlamova-Zabelina, E. I., Rapid Rotation of a Rigid Body around a Fixed Point in the Presence of a Non-Holonomic Constraint, *Vestn. Mosk. Univ. Ser. 1. Mat. Mekh.,* 1957, no. 6, pp. 25–34 (Russian).
23. Ziglin, S. L., On the Absence of an Additional First Integral in the Special Case of the G. K. Suslov Problem, *Russian Math. Surveys,* 1997, vol. 52, no. 2, pp. 434–435; see also: *Uspekhi Mat. Nauk,* 1997, vol. 52, no. 2(314), pp. 167–168.
24. Mahdi, A. and Valls, C., Analytic Non-Integrability of the Suslov Problem, *J. Math. Phys.,* 2012, vol. 53, no. 12, 122901, 8 pp.
25. Maciejewski, A. J. and Przybylska, M., Nonintegrability of the Suslov Problem, *J. Math. Phys.,* 2004, vol. 45, no. 3, pp. 1065–1078.
26. Fernandez, O. E., Bloch, A. M., and Zenkov, D. V., The Geometry and Integrability of the Suslov Problem, *J. Math. Phys.,* 2014, vol. 55, no. 11, 112704, 14 pp.
27. Kharlamova-Zabelina, E. I., Rigid Body Motion about a Fixed Point under Nonholonomic Constraint, *Tr. Donetsk. Industr. Inst.,* 1957, vol. 20, no. 1, pp. 69–75 (Russian).
28. Tatarinov, Ya. V., Separation of Variables and New Topological Phenomena in Holonomic and Nonholonomic Systems, *Tr. Sem. Vektor. Tenzor. Anal.,* 1988, vol. 23, pp. 160–174 (Russian).
29. Borisov, A. V., Mamaev, I. S., and Bizyaev, I. A., The Jacobi Integral in Nonholonomic Mechanics, *Regul. Chaotic Dyn.,* 2015, vol. 20, no. 3, pp. 383–400.
30. Bolsinov, A. V., Borisov, A. V., and Mamaev, I. S., Rolling of a Ball without Spinning on a Plane: The Absence of an Invariant Measure in a System with a Complete Set of Integrals, *Regul. Chaotic Dyn.,* 2012, vol. 17, no. 6, pp. 571–579.
31. Borisov, A. V., Mamaev, I. S., and Bizyaev, I. A., The Hierarchy of Dynamics of a Rigid Body Rolling without Slipping and Spinning on a Plane and a Sphere, *Regul. Chaotic Dyn.,* 2013, vol. 18, no. 3, pp. 277–328.
32. Borisov, A. V. and Mamaev, I. S., *Dynamics of a Rigid Body: Hamiltonian Methods, Integrability, Chaos*, 2nd ed., Izhevsk: R&C Dynamics, Institute of Computer Science, 2005 (Russian).

33. Bizyaev, I. A., Borisov, A. V., and Mamaev, I. S., The Dynamics of Nonholonomic Systems Consisting of a Spherical Shell with a Moving Rigid Body Inside, *Regul. Chaotic Dyn.,* 2014, vol. 19, no. 2, pp. 198–213.
34. Arnol'd, V. I., Kozlov, V. V., and Neĭshtadt, A. I., *Mathematical Aspects of Classical and Celestial Mechanics,* 3rd ed., Encyclopaedia Math. Sci., vol. 3, Berlin: Springer, 2006.
35. Kozlov, V. V., On the Existence of an Integral Invariant of a Smooth Dynamic System, *J. Appl. Math. Mech.,* 1987, vol. 51, no. 4, pp. 420–426; see also: *Prikl. Mat. Mekh.,* 1987, vol. 51, no. 4, pp. 538–545.
36. Benettin, G., Galgani, L., Giorgilli, A., and Strelcyn, J.-M., Lyapunov Characteristic Exponents for Smooth Dynamical Systems and for Hamiltonian Systems: A Method for Computing All of Them: P. 1: Theory; P. 2: Numerical Application, *Meccanica,* 1980, vol. 15, pp. 9–30.
37. Borisov, A. V., Jalnine, A. Yu., Kuznetsov, S. P., Sataev, I. R., and Sedova, J. V., Dynamical Phenomena Occurring due to Phase Volume Compression in Nonholonomic Model of the Rattleback, *Regul. Chaotic Dyn.*, 2012, vol. 17, no. 6, pp. 512–532.
38. Pikovsky, A. and Topaj, D., Reversibility vs. Synchronization in Oscillator Latties, *Phys. D,* 2002, vol. 170, pp. 118–130.
39. Roberts, J. A. G. and Quispe, G. R. W., Chaos and Time-Reversal Symmetry. Order and Chaos in Reversible Dynamical Systems, *Phys. Rep.*, 1992, vol. 216, nos. 2–3, pp. 63–177.
40. Kazakov, A. O., On the Chaotic Dynamics of a Rubber Ball with Three Internal Rotors, *Nonlinear Dynamics & Mobile Robotics*, 2014, vol. 2, no. 1, pp. 73–97.
41. Rocard, Y., *L'instabilité en mécanique: Automobiles, avions, ponts suspendus,* Paris: Masson, 1954.
42. Neimark, Ju. I. and Fufaev, N. A., *Dynamics of Nonholonomic Systems*, Trans. Math. Monogr., vol. 33, Providence, R.I.: AMS, 1972.
43. García-Naranjo, L. C., Maciejewski, A. J., Marrero, J. C., and Przybylska, M., The Inhomogeneous Suslov Problem, *Phys. Lett. A,* 2014, vol. 378, nos. 32–33, pp. 2389–2394.
44. Fassò, F. and Sansonetto, N., Conservation of Energy and Momenta in Nonholonomic Systems with Affine Constraints, *Regul. Chaotic Dyn.,* 2015, vol. 20, no. 4, pp. 449–462.
45. Bolsinov, A. V., Borisov, A. V., Mamaev, I. S., Geometrisation of Chaplygin's reducing multiplier theorem, *Nonlinearity*, 2015, vol. 28, no. 7, pp. 2307–2318.